DOI: 10.1002/chem.200500955

In Situ Spectroelectrochemical Studies on Ladder-Type Oligomers in Solution and the Solid State

Peter Rapta,*[a, b] Niels Schulte,[c] A. Dieter Schlüter,[c, d] and Lothar Dunsch*[a]

Abstract: A series of thermally stable fluoranthenopyracylene oligomers with extended π conjugation were studied by in situ ESR-UV/Vis/NIR spectroelectrochemistry with respect to their application in devices such as organic light-emitting diodes and field-effect transistors. The oligomers are both soluble in *o*-dichlorobenzene and form thin films by evaporation in the temperature range of 300–500 °C in vacuum. Their electrochemical behavior was studied in reduction (n doping) and oxidation (p doping) under standard voltammetric and thin-layer conditions. The HOMO and LUMO energies and the band gaps of all compounds under study were estimated from both electrochemical and UV/Vis/NIR spectroscopic data. The fluorene-type oligomers $\mathbf{A_2}$–$\mathbf{A_6}$ and $\mathbf{B_2}$ bearing flexible alkyl chains exhibit both reversible multistep reductions and oxidations. The spectroelectrochemistry indicates substantial differences in delocalization of the positive and negative charges in these ladder-type oligomers. The formation of doubly charged σ dimers was observed for the first time for both the radical anion and radical cation of the same molecule ($\mathbf{B_1}$). The redox behavior of the oligomers was studied in the solid state and in solution.

Keywords: electrochemistry · EPR spectroscopy · radical ions · redox chemistry · UV/Vis spectroscopy

Introduction

Organic charge-transport layers are the main component of organic devices. Though they play a key role in the function of the devices, their mode of operation on a molecular level, especially with regard to long-term stability, is not yet fully understood. To gain a better understanding of the complex electrochemical, chemical, and physical aspects involved, it is important to determine their electronic state. Our approach is to first understand the optical and redox properties such as molecular orbital energies (HOMO, SOMO, LUMO), reversible charge transfer, radical-ion stability, and dimer formation of the individual π-conjugated organic molecules which constitute the layer. This can be approached by a combination of cyclic voltammetry and UV/Vis/NIR and ESR spectroscopy,[1] which provides access to all above-mentioned properties from the spectroelectrochemical data. Second, the packing of these constituents and its influence on charge-transfer processes and stabilization of charged states in the layer must be understood.[2] Third, it is necessary to investigate the role of the interface between the organic layer and the metal electrode, not only with respect to energetics, but more importantly also to the detailed mechanism of charge injection.[3] All these aspects must be investigated for both electron- and hole-transporting layers, as both are equally important for the operation of a device.

As most of the organic materials are of the p type, n-type materials are urgently needed as components, for example, in photovoltaic devices.[4] We selected fluorene-type oligomers[5] of general structures **A** and **B** (Scheme 1) as model structures for systematic investigation of the above-mentioned aspects, as they exhibit both reversible reduction (n doping) and oxidation (p doping) similar to fluorene-based molecules.[6] They have a two-dimensionally extended π-conjugated structure and carry flexible alkyl chains that keep

[a] Dr. P. Rapta, Prof. L. Dunsch
Leibniz Institute for Solid State and Materials Research Dresden
Helmholtzstrasse 20, 01069 Dresden (Germany)
Fax: (+49) 351-4659-811
E-mail: peter.rapta@stuba.sk
L.Dunsch@ifw-dresden.de

[b] Dr. P. Rapta
Slovak University of Technology
Radlinského 9, SK-812 37 Bratislava (Slovak Republic)
Fax: (+421) 2-52493-198

[c] Dr. N. Schulte, Prof. A. D. Schlüter
Institut für Chemie, Freie Universität Berlin
Takustrasse 3, 14195 Berlin (Germany)

[d] Prof. A. D. Schlüter
New address:
Swiss Federal Institute of Technology
Department of Materials, Institute of Polymers
ETH-Hönggerberg, 8093 Zürich (Switzerland)

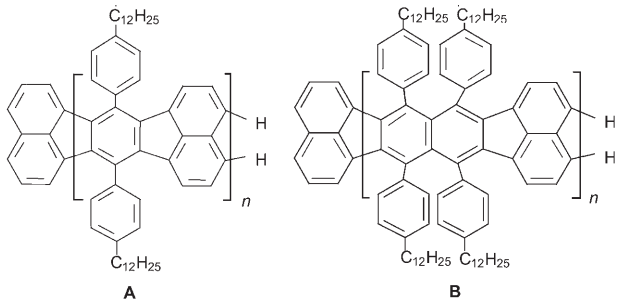

Scheme 1. Chemical structures of fluoranthenopyracylene compounds **A** and **B** (**A$_1$**, **B$_1$**: $n=1$; **A$_2$**, **B$_2$**: $n=2$; **A$_3$**: $n=3$, **A$_4$**: $n=4$; **A$_6$**: $n=6$).

them molecularly disperse in solution. Furthermore, they lead to amorphous layer structures, which should show better long-term stability. Recently, we began to study this area by investigating charge injection into compounds **A** by temperature-dependent in situ ESR-UV/Vis/NIR spectroscopy[5] and found a considerable influence of the extent of the π system on the tendency of radical anions to dimerize. Stimulated by this interesting finding, we set out to explore the hole-injection properties of such molecules and to substantially broaden the entire study by using compounds of type **B**. Owing to the slight extension of the π-conjugated system in **B** compared with **A**, the corresponding radical cations become persistent in solution already for monomeric structure **B$_1$**, which makes studying reversible dimerization for both reduction and oxidation of the same molecule possible. The influence of oligomer length on the stabilization of charged states in compounds **A$_n$** ($n=1$, 2, 4, 6) and **B$_n$** ($n=1$, 2; Scheme 1), both in solution and the solid state, with respect to applications in electroluminescence and photovoltaics is discussed.

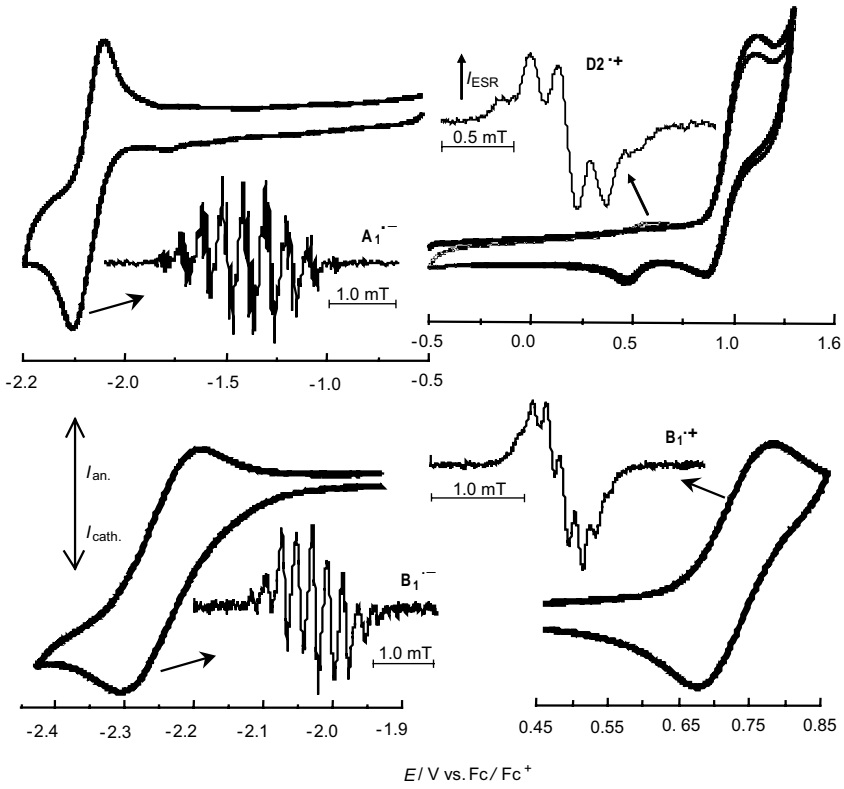

Figure 1. Cyclic voltammograms of **A$_1$** and **B$_1$** in 0.1 mol L^{-1} TBABF$_4$/*o*-DCB (scan rate 0.2 V s^{-1}) and ESR spectra of radical ions generated electrochemically in situ at the first redox peak.

Results and Discussion

Studies in solution

ESR-UV/Vis/NIR spectroelectrochemistry: The UV/Vis/NIR and the ESR spectra measured for reduction of **A$_1$**, **A$_2$**, **B$_1$**, **B$_2$** and oxidation of **A$_2$**, **B$_1$**, **B$_2$** demonstrate that one-electron transfer results in initial formation of radical ions, as shown illustratively in Figures 1 and 2 for **A$_1$** and **B$_1$**. The spectroelectrochemical results for all compounds under study are summarized in Tables 1–3. The visible spectra of the radical ions of **B$_1$** show the expected bands at $\lambda_{max}=$ 595 nm for radical anion **B$_1^{\bullet-}$** and $\lambda_{max}=584$ nm for radical cation **B$_1^{\bullet+}$**, as was verified by simultaneously applying ESR spectroscopy. Additionally, during oxidation in the potential region of the first electron transfer, a new band at 680 nm for reduction and 660 nm for oxidation of **B$_1$** was observed. The intensity of this latter band increases during reduction or oxidation (Figure 2). On the back scan this band disappears simultaneously with the bands characteristic of radical ions, and the UV/Vis spectrum of neutral **B$_1$** is recovered; this indicates reversibility of redox and chemical processes both for oxidation and reduction of **B$_1$**. The species associated with this additional band is ESR-silent and must therefore be formed by a chemical follow-up reaction of the radical ions. This is attributed to the formation of doubly charged σ dimers, which are clearly reversibly formed. This behavior applies both to the radical anion and the radical cation of the same molecule **B$_1$**, which for one and the same compound is a new finding. Though the dimerization of radical ions has already been observed for short π-conjugated molecules[2] and was to some extent discussed in our previous work on compounds of type **A$_n$**,[5] the reversible dimeri-

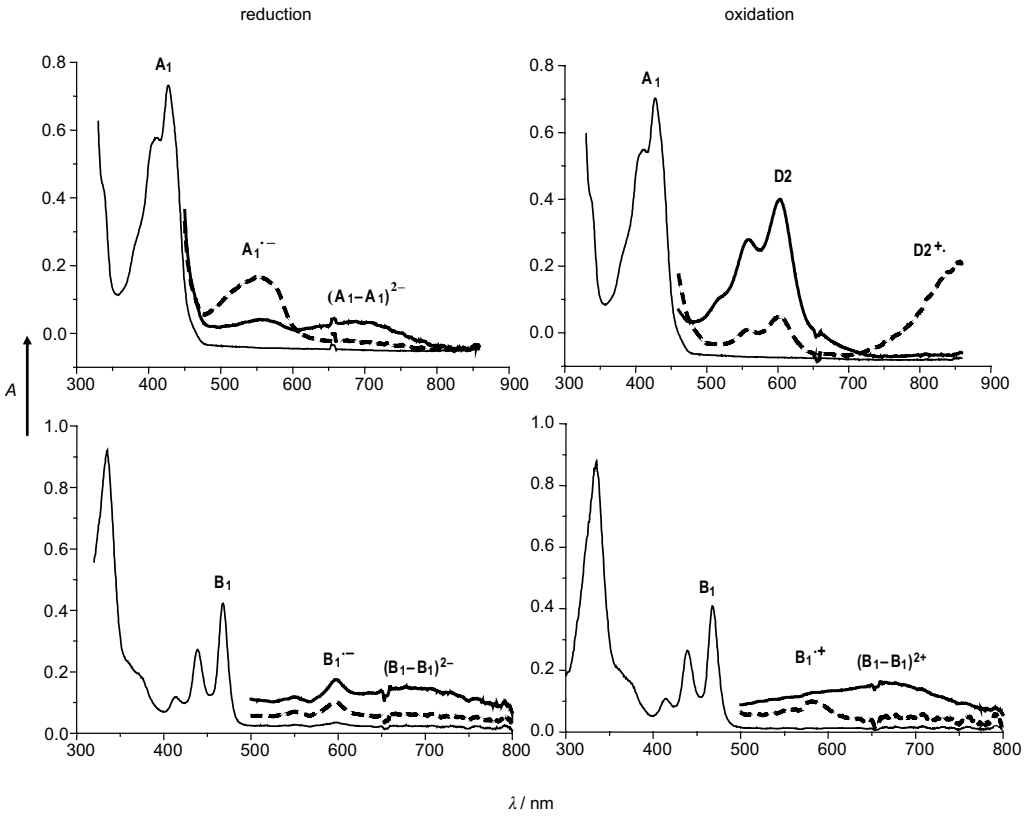

Figure 2. UV/Vis spectra of $\mathbf{A_1}$ and $\mathbf{B_1}$ (thin solid lines) and visible spectra of their products (dashed lines: radical ions, broad solid lines: σ dimers; expanded for clarity) formed on anodic oxidation and cathodic reduction in the region of the first electron transfer in 0.1 mol L^{-1} $TBABF_4$/*o*-DCB solutions.

Table 1. Cyclic voltammetry data [V vs Fc/Fc^+] for **A** and **B** in reduction and oxidation (*o*-DCB + 0.1 mol L^{-1} $TBABF_4$, scan rate 0.2 V s^{-1}). $E_{1/2}(\text{red.})^i$ and $E_{1/2}(\text{ox.})^i$ are the half-wave potentials for the first ($i=1$) and the second ($i=2$) redox step for reduction and oxidation respectively.

Compound	$E_{1/2}(\text{red})^1$	$E_{1/2}(\text{red})^2$	$E_{1/2}(\text{ox})^1$	$E_{1/2}(\text{ox})^2$	$E_{1/2}(\text{ox})^1-E_{1/2}(\text{red})^1$	$E_{1/2}(\text{red})^1-E_{1/2}(\text{red})^2$	$E_{1/2}(\text{ox})^2-E_{1/2}(\text{ox})^1$
$\mathbf{A_1}$	−2.09	–	1.02[a]	–	3.11	–	–
$\mathbf{A_2}$	−1.70	−1.97	0.77	1.17	2.47	0.27	0.40
$\mathbf{A_3}$	−1.66	−1.82	0.67	0.95	2.33	0.15	0.30
$\mathbf{A_4}$	−1.54	−1.65	0.64	0.89	2.18	0.11	0.25
$\mathbf{A_6}$	−1.5	−1.5	0.63	0.76	2.13	0	0.13
$\mathbf{B_1}$	−2.25	–	0.74	–	2.99	–	–
$\mathbf{B_2}$	−1.98	−2.20	0.62	0.95	2.60	0.22	0.33

[a] Irreversible first oxidation step.

Table 2. UV/Vis/NIR spectroscopic data for compounds **A** and **B** and their anions and cations in 0.1 mol L^{-1} $TBABF_4$/*o*-DCB solutions.[a]

Compound	λ_{max} [nm (eV)]	HOMO [eV]	LUMO [eV]	λ^1_{max}(anion) [nm]	λ^1_{max}(cation) [nm]	λ^2_{max}(anion) [nm]	λ^2_{max}(cation) [nm]
$\mathbf{A_1}$	429 (2.9)	−5.82	−2.71	555	–	1390	–
$\mathbf{A_2}$	496 (2.5)	−5.57	−3.10	660	593 (670, 770)	(1120) 1310	(1215) 1520
$\mathbf{A_3}$	532 (2.33)	−5.44	−3.13	706	645 (721)	(1290) 1414	(1308, 1450) 1650
$\mathbf{A_4}$	546 (2.27)	−5.44	−3.26	728	668 (744)	(1476) 1615	(1347) 1494[b]
$\mathbf{A_6}$	565 (2.19)	−5.43	−3.25	732 (850)	668 (760)	(1492) 1630	ca. 1700
$\mathbf{B_1}$	468 (2.65)	−5.83	−2.74	595	584	_[b]	_[b]
$\mathbf{B_2}$	545 (2.27)	−5.61	−3.11	(673) 735	(658) 725	(1215) 1440	1400[b]

[a] HOMO and LUMO energies were determined from voltammetric and spectroscopic data, by assuming the HOMO energy for Fc/Fc^+ to be −4.8 eV with respect to the zero vacuum level. λ_{max} is the maximum of the main band in the visible region of the neutral compound, λ^1_{max} the maximum of the main band in the visible region of the corresponding radical ion, and λ^2_{max} the maximum of the main band in the NIR region of the corresponding radical ion; in parentheses: maxima of the most intense shoulders). [b] Low-intensity signal or not observed.

Table 3. ESR data of anions and cations of compounds **A** and **B**.

Compound	Hyperfine splitting [mT] (anions)	Hyperfine splitting [mT] (cations)
$\mathbf{A_1}$	$4a_H=0.055$, $4a_H=0.277$, $4a_H=0.298$	singlet ($\mathbf{D1^{\cdot+}}$) and $4a_H=0.041$, $4a_H=0.20$ ($\mathbf{D2^{\cdot+}}$)[a]
$\mathbf{A_2}$	$4a_H=0.059$	singlet ($\Delta H_{p-p}=0.22$ mT)
$\mathbf{A_3}$	weak singlet	singlet ($\Delta H_{p-p}=0.18$ mT)
$\mathbf{A_4}$	weak singlet	singlet ($\Delta H_{p-p}=0.18$ mT)
$\mathbf{A_6}$	no signal	singlet ($\Delta H_{p-p}=0.18$ mT)
$\mathbf{B_1}$	$4a_H=0.04$, $4a_H=0.247$, $4a_H=0.272$	$4a_H=0.026$, $8a_H=0.15$
$\mathbf{B_2}$	$2a_H=0.26$, $4a_H=0.19$	singlet ($\Delta H_{p-p}=0.25$ mT)

[a] Two overlapping ESR spectra.

zation of both radical cation and radical anion of the same molecule is new. The slight extension of the π system in $\mathbf{B_1}$ as compared to $\mathbf{A_1}$ leads to stabilization of the corresponding radical cation $\mathbf{B_1}^{\cdot+}$, which renders its dimerization reversible (Scheme 2).

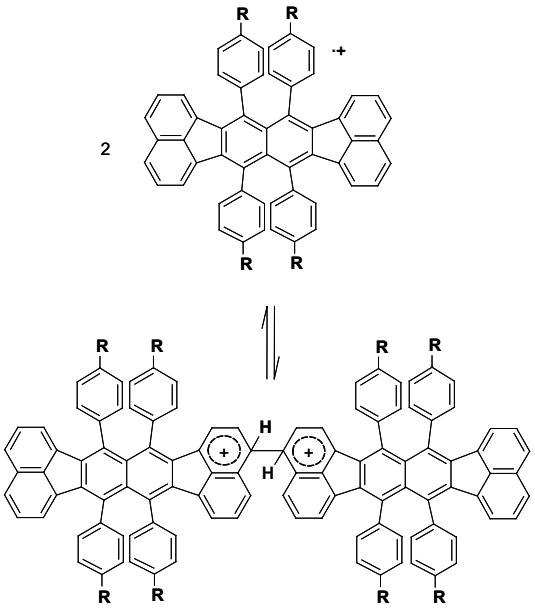

Scheme 2. Reaction scheme of the reversible dimerization of $\mathbf{B_1}^{\cdot+}$ ($R=C_{12}H_{25}$).

An electrochemical oxidation $\mathbf{A_1}$ does not show this reversible dimerization (Figure 1, right), and a more complex and irreversible follow-up chemistry leads to the new dimers **D1** and **D2**. A mechanistic proposal for this follow-up reaction is presented in Scheme 3. It involves formation of a perylene subunit by elimination of protons, which is based on similar observations for diphenylbenzo[*k*]fluoranthenes[7] and further supported by the following findings. On oxidation of $\mathbf{A_1}$ two different ESR spectra with corresponding optical bands at 670 and 928 nm are observed in situ (Figure 3). They are attributed to the radical cations of dimers **D1** and **D2**, respectively, which are formed subsequently by coupling of the electrogenerated radical cations. Initially, a neutral dimer **D1** with a single bond between the two monomer units is formed in a first coupling step. Similar to what is observed for dimeric diphenylbenzo[*k*]fluoranthenes, oxidation of just-formed dimer **D1** leads to localization of the charge on one part of the molecule in $\mathbf{D1}^{\cdot+}$, and the oxidation potential is similar to the oxidation potential of monomer $\mathbf{A_1}$, as the two monomers are probably twisted at the central chemical bond.[7] The ESR line with unresolved splitting observed in the initial stages of $\mathbf{A_1}$ oxidation (Figure 3a) is assigned to the less stable radical cation $\mathbf{D1}^{\cdot+}$. On repeating the potential cycle a new reversible redox couple was observed at a much lower oxidation potential (ca. 0.6 V vs Fc/Fc^+) compared to $\mathbf{A_1}$ and **D1** (ca. 1.0 V vs Fc/Fc^+), which indicates formation of the second

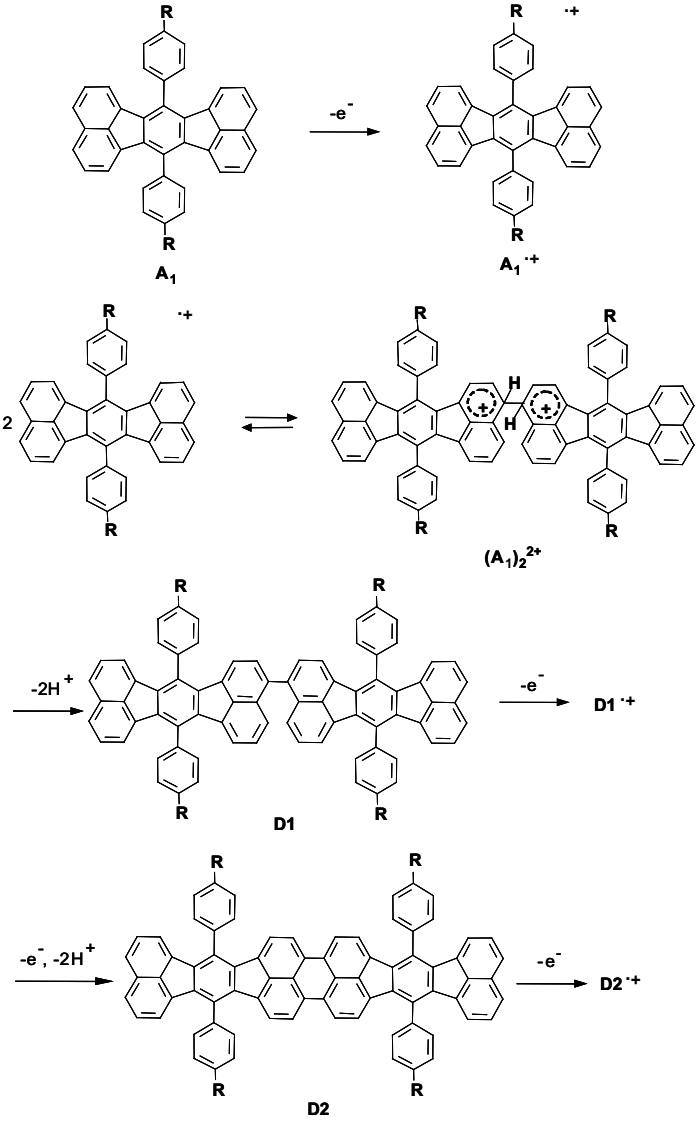

Scheme 3. Reaction scheme of the irreversible dimerization of $\mathbf{A_1}^{\cdot+}$ ($R=C_{12}H_{25}$).

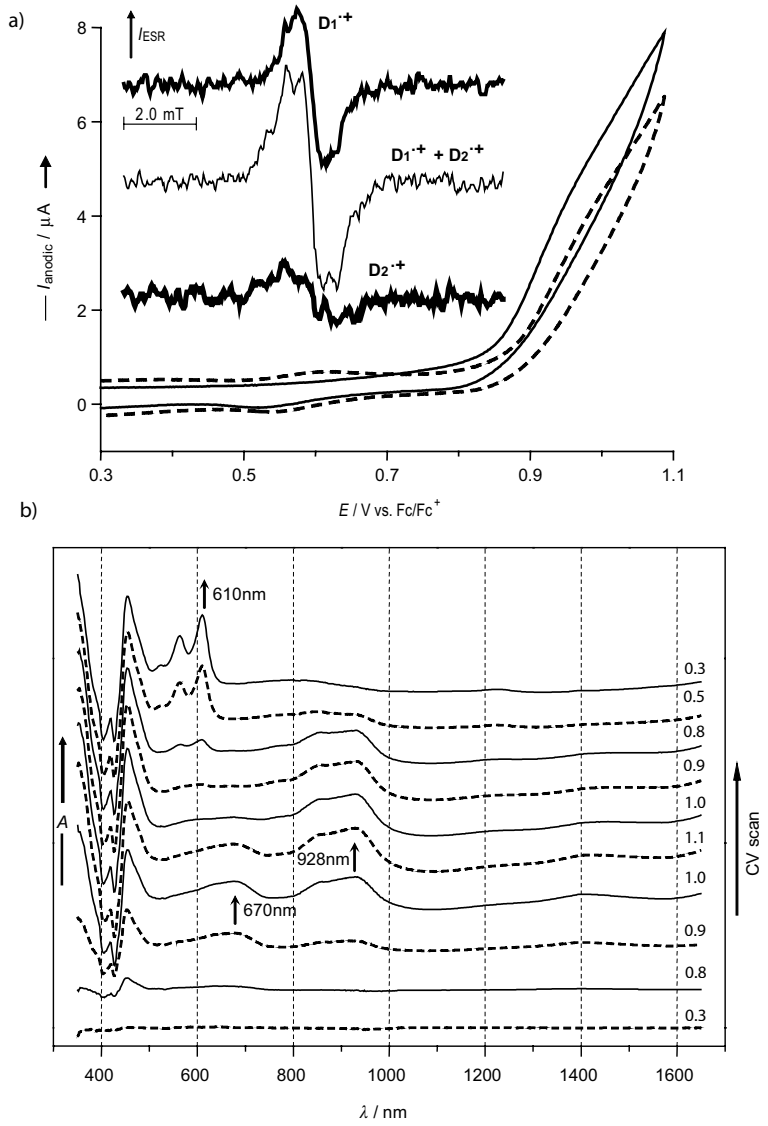

Figure 3. In situ spectroelectrochemistry of $\mathbf{A_1}$ oxidation in $TBABF_4$/*o*-DCB solution. a) Cyclovoltammetric curves (solid line: first scan, dashed line: second scan; scan rate 3 $mV\,s^{-1}$) and representative ESR spectra observed during oxidation. b) UV/Vis/NIR spectra recorded during the first cyclovoltammetric scan (curve parameter: potential [V] vs Fc/Fc^+; the broadened voltammetric peaks are due to the large ohmic drop in the flat ESR cell).

dimer **D2** by intramolecular coupling of oxidized **D1**. At this stage of oxidation a stable radical which can be simulated by splitting constants $4a_H = 0.041$, $4a_H = 0.199$ mT was observed. These ESR splitting parameters support the presence of a new perylene moiety in the molecule, and therefore the second ESR spectrum can be attributed to the radical cation $\mathbf{D2^{\cdot+}}$ [see also the well-defined ESR spectrum of $\mathbf{D2^{\cdot+}}$ which was observed on exhaustive in situ oxidation of $\mathbf{A_1}$ with a large platinum mesh (Figure 1, right)]. Formation of a stable perylene radical cation is known from literature data;[8] the unpaired spin density is partially localized over this perylene ring (8 protons). In addition, the back scan to the initial potential results in a new ESR-silent structure with an optical band at 610 nm (Figure 3b), which is similar in its absorption pattern to perylene.[9] On repeating the voltammetric scan a new oxidation peak was observed at 0.6 V versus Fc/Fc^+, while the decrease in the optical band at 610 nm (assigned to **D2**) is accompanied by an increase in the band at 928 nm and in the intensity of the ESR spectrum assigned to $\mathbf{D2^{\cdot+}}$. These spectroscopic results confirm the suggested dimerization mechanism for $\mathbf{A_1}$ (Scheme 3).

Compounds $\mathbf{A_2}$ and $\mathbf{B_2}$, the next higher homologues of $\mathbf{A_1}$ and $\mathbf{B_1}$, give stable radical ions in the first electron transfer to a large extent. As no temperature dependence of UV/Vis/NIR spectra of radical ions were observed for these compounds, formation of π or σ dimers is negligible even down to a temperature of 260 K (see Figure 4a), at which the dimers should be more stable both for radical anions and radical cations. Generally, the optical spectra of π-dimerized radical ions are strongly temperature dependent.[2] Also, no irreversible dimerization according to Scheme 3 is observed. The higher homologues show similar behavior.

For all compounds under study the optical, redox, and ESR results, along with the HOMO–LUMO energies determined from cyclovoltammetric and optical data (taking the LUMO value versus vacuum level of −4.8 eV for ferrocene as internal potential standard), are summarized in Tables 1–3. The increase in π-conjugation length of $\mathbf{A_1}$–$\mathbf{A_6}$ and $\mathbf{B_1}$, $\mathbf{B_2}$ is reflected by the bathochromic shift of the absorption bands. This shift already levels off for hexamer $\mathbf{A_6}$. The reductive redox behavior of the tetramer $\mathbf{A_4}$ and the hexamer $\mathbf{A_6}$ with a large π system gives a cyclovoltammetric response similar to that of oligo(*p*-phenylenevinylene)s.[10] The redox potentials shift towards lower energies and the potential difference between subsequent redox states decreases. For $\mathbf{A_6}$ the potential difference between the first two redox states even vanishes (Table 1). No ESR signal was observed in the reduction of $\mathbf{A_6}$, while only a very weak, single ESR line was found in the reduction of $\mathbf{A_4}$. The optical absorption bands can be at-

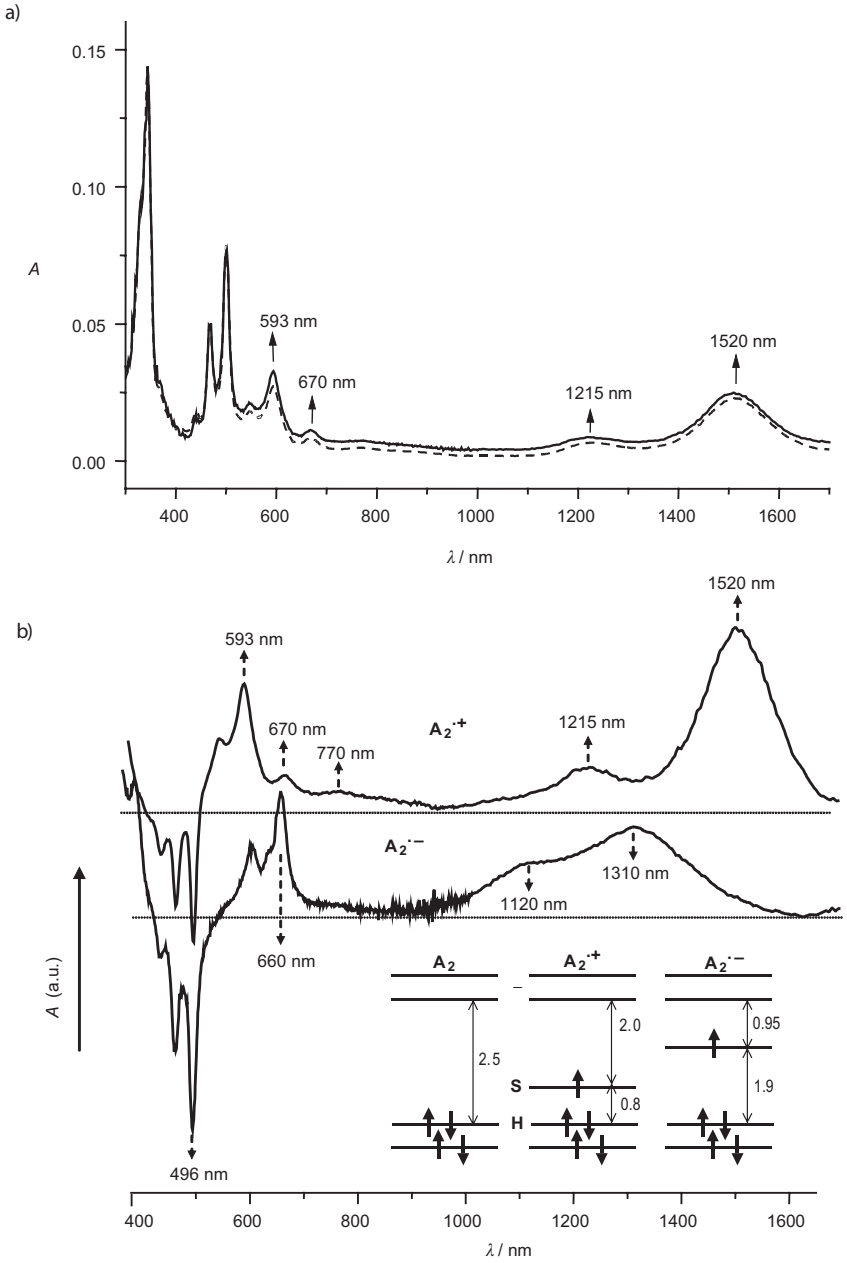

Figure 4. a) UV/Vis/NIR spectra observed during anodic oxidation of $\mathbf{A_2}$ at different temperatures (——: 300 K, -----: 262 K) in $TBABF_4$/*o*-DCB solution in the region of the first electron transfer. b) UV/Vis/NIR absorption spectra of radical anion and radical cation of $\mathbf{A_2}$ generated electrochemically in $TBABF_4$/*o*-DCB solutions at room temperature (inset: schematic energy diagram of neutral, positively charged, and negatively charged $\mathbf{A_2}$; only the most intense transitions [eV] are shown for clarity).

tributed to ESR-silent, doubly charged structures which are formed preferably in the oligomer chain on successive transfer of two electrons.[11] Here formation of an interchain dimer is negligible because of the higher stability of the dianion.

In the oxidation of structures $\mathbf{A_2}$–$\mathbf{A_6}$ the redox-potential separation between the first one-electron transfer steps is higher than in the case of their reduction, and this indicates differences in delocalization of the positive and negative charges in the conjugated system. Thus, for $\mathbf{A_6}$ oxidation the potential difference of the first two electron transfers is 130 mV. The cyclic voltammetric curve of $\mathbf{A_4}$ oxidation shows a relatively even spacing of about 250 mV up to the fourth electron transfer, a behavior which is similar to fullerene reductive voltammetry and indicates delocalized orbitals.[12] For all homologues $\mathbf{A_2}$–$\mathbf{A_6}$ we observed an intense single ESR line in the region of the first oxidation peak, in contrast to the anions of $\mathbf{A_3}$–$\mathbf{A_6}$ (Table 3). This behavior is due to the distinct potential difference of the first two oxidation peaks for compounds $\mathbf{A_2}$–$\mathbf{A_6}$, which do not show superposition of the first and second electron transfers. The ESR spectrum of the radical cation $\mathbf{A_2}^{\bullet+}$ shows a single rather sharp line (ΔH_{p-p} = 0.22 mT), in contrast to the radical anion $\mathbf{A_2}^{\bullet-}$. The same holds true for the homologues $\mathbf{A_3}$–$\mathbf{A_6}$ ($\Delta H_{p-p} \approx 0.18$ mT; Table 3). In addition, the significantly different g values observed, for example, for radical anion $\mathbf{A_2}^{\bullet-}$ (2.0052) and radical cation $\mathbf{A_2}^{\bullet+}$ (2.0026) confirm different delocalization of positive and negative charges. The unresolved ESR signal points to extended delocalization of the unpaired electron in the radical cations of these compounds and formation of mobile charge carriers, as the ESR line width of polyconjugated systems can be taken as a measure of charge-carrier mobility.[13]

The UV/Vis/NIR pattern of the species formed on oxidation of $\mathbf{A_2}$–$\mathbf{A_6}$ and $\mathbf{B_1}$, $\mathbf{B_2}$ is similar to that observed in their reductive electrochemistry, as illustrated for reduction and oxidation of $\mathbf{A_2}$ in Figure 4b. Generally, in the first stages of oxidation two characteristic absorption bands of ESR-active species (polaron-like structures) dominate the optical range (Table 2). In the higher energy absorption, a rich vibrational fine structure and a similar pattern for all structures (500–800 nm region) was found. This transition can be assigned to excitation of the unpaired electron from SOMO (S) to LUMO (L), whereas the band observed in the NIR region is caused by excitation

from HOMO (H) to SOMO (see the simplified energy diagram in Figure 4b). For anions the transition at higher wavelengths can be assigned to excitation of the unpaired electron from SOMO to LUMO, as was observed in oligomeric extended π systems.[14] The smaller energy difference between HOMO and SOMO in cations compared with that between SOMO and LUMO in anions indicates different charge distributions in positively and negatively charged structures **A** and **B**, as was already indicated by cyclovoltammetric and ESR experiments. Furthermore, a characteristic red shift was observed for both anions and cations, which increases with increasing chain length (Table 2). The pattern of the lower energy transitions (NIR region) is more complex, but a red shift of this band is observable. Thus, by increasing the chain length the NIR bands become much broader, reflecting the increase in charge delocalization. In the case of cations both visible and NIR bands are broader compared to anions (e.g., see Figure 4b), and this confirmed greater delocalization in p-doped states.

Thin-layer spectroelectrochemistry: In a standard spectroelectrochemical setup with a platinum mesh as working electrode, for which semi-infinite diffusion conditions must be considered, comproportionation/disproportionation reactions will make the redox mechanism of the studied fluoranthenopyracylene structures more complicated. Thus, a strong increase in spin concentration occurs in the second electron transfer. The increase in spin number is attributed to a comproportionation between the starting material and the diionic species to produce radicals ($A^{2+} + A \rightarrow 2\,A^{\bullet+}$). To avoid this problem of interference by the starting material, we used a spectroelectrochemical cell with thin-layer behavior. In our cell construction the advantages of laminated electrodes[15] are combined with those of lithographic/galvanic (LIGA) spectroelectrochemical cells by using microstructured electrode materials.[16] As standard laminated working electrode a gold LIGA structure having honeycombed microstructure with well-defined hexagonal holes was used. The space between the electrode surface and the flat wall of the ESR cell is sufficiently small to create thin-layer conditions at lower scan rates. Similar experiments with this cell construction were successfully applied to the spectroelectrochemistry of pyrrole hexamer by using a gold micromesh electrode.[17] The gold LIGA electrodes used in this study ensure stable handling during the measurements due to their mechanical stability. The larger active and well-defined metal electrode surface of the LIGA structure results in a better electrochemical response compared to commercially available gold micromeshes, which is advantageous for detailed mechanistic studies. We applied this electrode especially in reduction and oxidation of trimeric $\mathbf{A_3}$ to distinguish between very similar patterns of optical spectra of mono and doubly charged $\mathbf{A_3}$ (see below).

The spectroelectrochemical behavior of trimer $\mathbf{A_3}$ on reduction confirms the existence of well-defined thin-layer conditions in the spectroelectrochemical cell (Figure 5). The $\mathbf{A_3}$ dianion exhibits a dominant absorption band in the NIR region at 1250 nm that points to a bipolaronic structure.

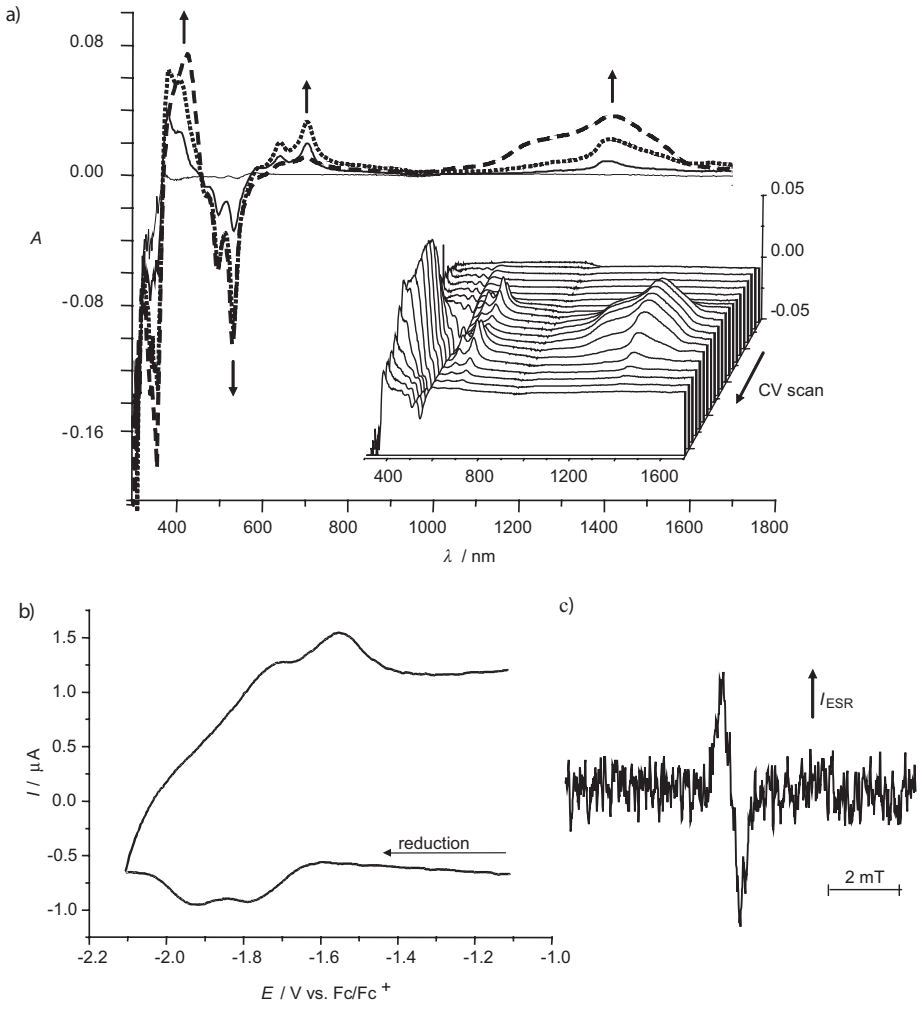

Figure 5. In situ ESR-UV/Vis/NIR spectrocyclovoltammogram of $\mathbf{A_3}$ reduction in 0.1 mol L^{-1} $TBABF_4$/*o*-DCB. a) Representative difference UV/Vis/NIR spectra (inset: all measured optical spectra in a 3D plot) recorded during b) the cyclovoltammetric scan along with c) the characteristic ESR spectrum observed at the maximum of the first cyclovoltammetric peak (scan rate 3 mV s^{-1}, laminated gold LIGA working electrode).

This band is only slightly blue-shifted from the NIR band corresponding to radical anion $\mathbf{A_3}^{\bullet-}$ The visible absorption band (ca. 700 nm) is considerably weaker and slightly broader than that of the $\mathbf{A_3}$ radical anion. Similar phenomena were observed in the oxidation of $\mathbf{A_3}$ (not shown), although some important differences were found. The difference between the first and the second voltammetric peaks is much higher than in $\mathbf{A_3}$ reduction. The ESR signal of the radical cation is therefore considerably stronger due to higher radical concentrations. No dicationic species are formed at the potential of the first electron transfer; the second electron transfer is clearly separate. Similar to the results for $\mathbf{A_3}$ reduction, the NIR band of the radical cation has a vibronic pattern. Furthermore, a new absorption band at 1550 nm appears in the second electron transfer, while the ESR intensity decreases, as is expected for ESR-silent, doubly charged $\mathbf{A_3}$. In contrast to $\mathbf{A_3}$ reduction, the band in the visible region is also present in the region of the second electron transfer. Only a slight decrease in the intensity of this band was observed. The same phenomenon was found in thin-film spectroelectrochemistry of $\mathbf{A_2}$, where similar optical bands were observed in the first two one-electron oxidation peaks (see below). The bands of both the cation and dication are only slightly blue-shifted compared with the optical bands of the radical cation structure.

Studies in the solid state

Spectroelectrochemistry of solid films: A comparison of the solution and solid-state spectroelectrochemical behavior is of major importance with respect to the existence of intra- and interchain interactions between charged extended π systems. Thin solid films of compounds $\mathbf{A_1}$ and $\mathbf{A_2}$ were prepared by vacuum evaporation onto glass substrates coated with indium tin oxide (ITO) and studied by solid-state electrochemistry. For $\mathbf{A_1}$ and $\mathbf{A_2}$ the AFM images of the films and their UV/Vis absorption spectra in contact with acetonitrile (ACN) with $TBABF_4$ as supporting electrolyte are shown in Figure 6. Their UV/Vis spectra in *o*-dichlorobenzene (*o*-DCB) and dichloromethane (DCM) solutions are shown for comparison. Taking into account the difference in dipole moments for *o*-DCB ($\mu = 2.14$ D) and DCM ($\mu = 1.14$ D) the slight red shift of the optical band in *o*-DCB ($\lambda_{max} = 500$ nm) in comparison to DCM solutions ($\lambda_{max} = 495$ nm) confirms the π character of this optical transition in compounds $\mathbf{A_1}$ and $\mathbf{A_2}$.

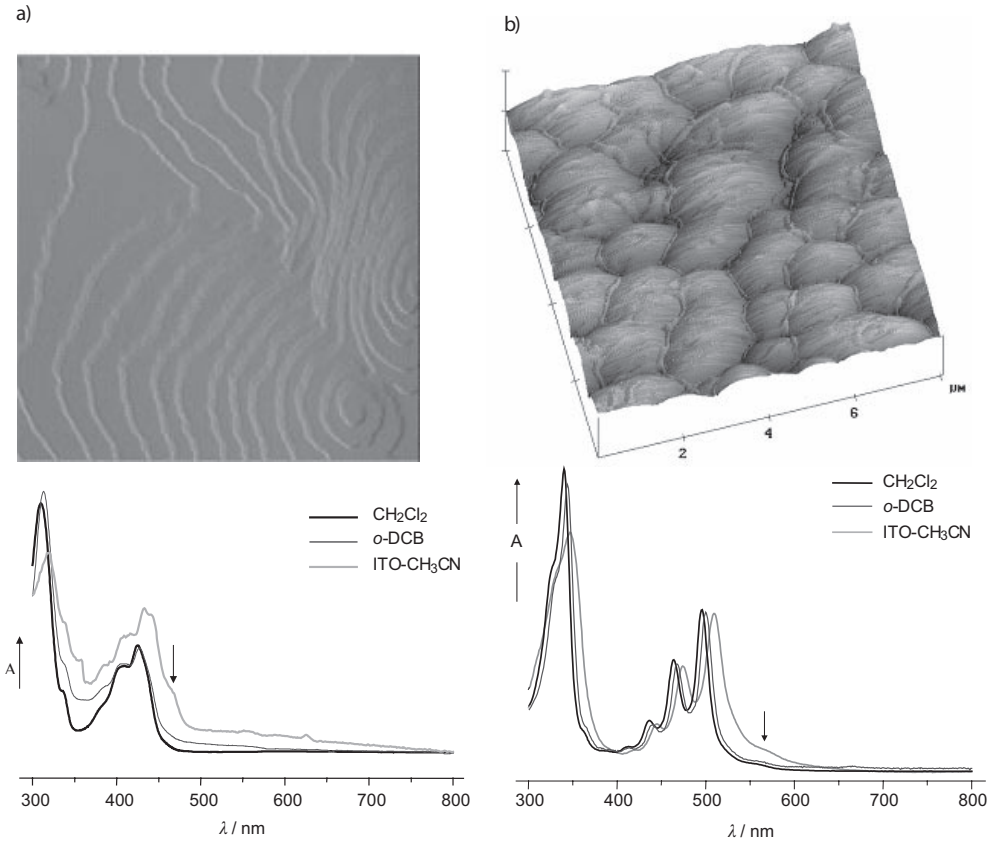

Figure 6. a) AFM image of a thin solid film of $\mathbf{A_1}$ prepared by vacuum evaporation onto ITO/glass substrate and UV/Vis spectra of $\mathbf{A_1}$ in *o*-dichlorobenzene and dichloromethane solution and of a thin solid film of $\mathbf{A_1}$ on ITO in contact with acetonitrile/0.1 mol L^{-1} $TBABF_4$ solution. b) AFM image of a thin solid film of $\mathbf{A_2}$ prepared by vacuum evaporation onto ITO/glass substrate and UV/Vis spectra of $\mathbf{A_2}$ in dichlorobenzene and dichloromethane solutions and of a thin solid film of $\mathbf{A_2}$ on ITO in contact with acetonitrile/0.1 mol L^{-1} $TBABF_4$ solution.

Pristine thin films of $\mathbf{A_1}$ and $\mathbf{A_2}$ deposited on ITO substrates underwent no changes in air or in contact with acetonitrile (negligible solubility in ACN was observed for all compounds under study). Therefore the observed red shift ($\lambda_{max} = 510$ nm) and the considerable line broadening are most likely caused by interactions of molecules in the solid state.[18] The lowest energy mode (arrows in Figure 6) indicates a molecular interaction in the samples. Especially the lowest energy mode for $\mathbf{A_1}$, which is resolved as a peak, reflects regular molecular aggregates in the amorphous film. This is also supported by AFM measurements, in which well-defined stepped structures are observed for $\mathbf{A_1}$ layers on ITO on the submicrometer scale (Figure 6a).

The spectroelectrochemistry of the solid films was studied in 0.1 mol L^{-1} $TBABF_4$/acetonitrile solutions. During cathodic reduction of the $\mathbf{A_1}$ film on ITO, new optical bands of the radical anion $\mathbf{A_1}^{\bullet-}$ and its reversibly formed σ dimer dianion $(\mathbf{A_1})_2^{2-}$ were found, similar to the solution spectroelectrochemistry of $\mathbf{A_1}$ (Figure 7a). Only a slight shift of the bands for both the radical anion and dimer (550 and 715 nm) and line broadening were observed in comparison to spectroelectrochemistry in *o*-DCB solutions (absorptions at 555 and 700 nm). Therefore, both the reduction behavior and the stabilization of negatively charged states of $\mathbf{A_1}$ are similar in solution and in the solid state. A more complex behavior was observed for oxidation of the $\mathbf{A_1}$ film (Figure 7b). As already described above for solution spectroelectrochemistry, oxidation of $\mathbf{A_1}$ results in complex chemical reactions leading to formation of dimers **D1** and **D2** (Scheme 3). Similarly, oxidation of the $\mathbf{A_1}$ solid film in acetonitrile leads to irreversible changes in the film and simultaneously the color of the film surface changes. A violet coloration was observed, similar to the anodic oxidation of $\mathbf{A_1}$ in dichlorobenzene. The same redox behavior on oxidation of $\mathbf{A_1}$ both in the film and in solution is strongly supported by in situ ESR spectroelectrochemistry of the $\mathbf{A_1}$ film in acetonitrile. Here similar ESR spectra were observed on oxidation as in solution spectroelectrochemistry (inset in Figure 7b). The line broadening and slight anisotropy of the ESR signal of the radicals of dimers **D** are due to the solid matrix. In contrast to solution UV/Vis spectroelectrochemistry, much broader unresolved optical bands in the region from 450 to 800 nm were found for the film (Figure 7b). This can be explained by the fact that the chemical follow-up reactions are not diffusion-controlled and the products formed are "trapped" in the film. Additionally, irreversible changes in the film cause strong changes in baseline of the spectra.

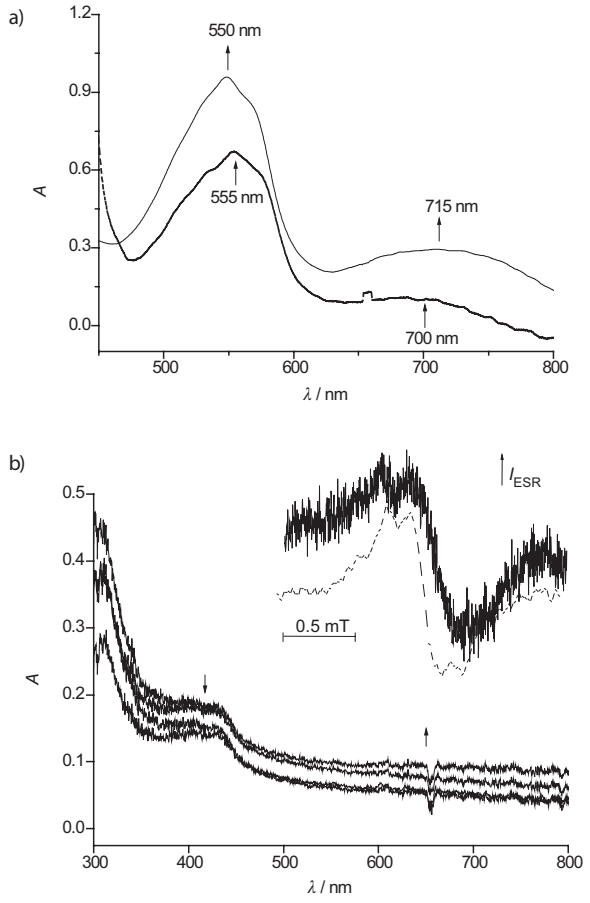

Figure 7. UV/Vis spectra of $\mathbf{A_1}$ deposited on ITO in 0.1 mol L^{-1} $TBABF_4$/ACN (solid lines) or in 0.1 mol L^{-1} $TBABF_4$/*o*-DCB solution (dashed lines) observed under a) cathodic reduction and b) anodic oxidation. Inset in b): ESR spectra observed during in situ anodic oxidation of $\mathbf{A_1}$ film in 0.1 mol L^{-1} $TBABF_4$/ACN (solid line) or in 0.1 mol L^{-1} $TBABF_4$/*o*-DCB solution (dashed line).

Further in situ ESR-UV/Vis/NIR solid-state spectroelectrochemical studies were therefore focused on the spectroelectrochemistry of $\mathbf{A_2}$ solid film, in which reversible redox processes are expected. The spectroelectrochemical response of the $\mathbf{A_2}$ thin layer on ITO shows two distinct oxidation steps (Figure 8a). Similar to solution electrochemistry, two well-defined waves at 1.55 and 1.70 V versus Ag pseudoreference electrode were observed, which are associated with spectral changes, as shown in Figure 8b and c. In the first anodic electron transfer two optical bands at 604 and 1490 nm were found which are characteristic of radical cation $\mathbf{A_2}^{\bullet+}$. Compared to spectroelectrochemistry in *o*-DCB these bands are slightly shifted (595 and 1510 nm). No remarkable changes in the shape of optical spectra and ESR intensity compared to solution spectroelectrochemistry were found. This confirms the absence of strong molecular interactions in the amorphous state of the solid films, which results in a negligible tendency for interchain dimer formation, similar to the behavior already observed in solution spectroelectrochemistry at lower temperatures. The lack of interchain dimerization is due to the influence of the bulky substituents, which reduces the intermolecular interactions even in the different redox states and increases the persistence of the amorphous state. In the thin solid films steric hindrance plays a crucial role, as these substituents are twisted out of plane of the planar part of the molecule, where most of spin density is located.[5] Consequently, they also hinder interaction between the two neighboring radical cations and thus block dimerization. This is similar to findings for thienylene-

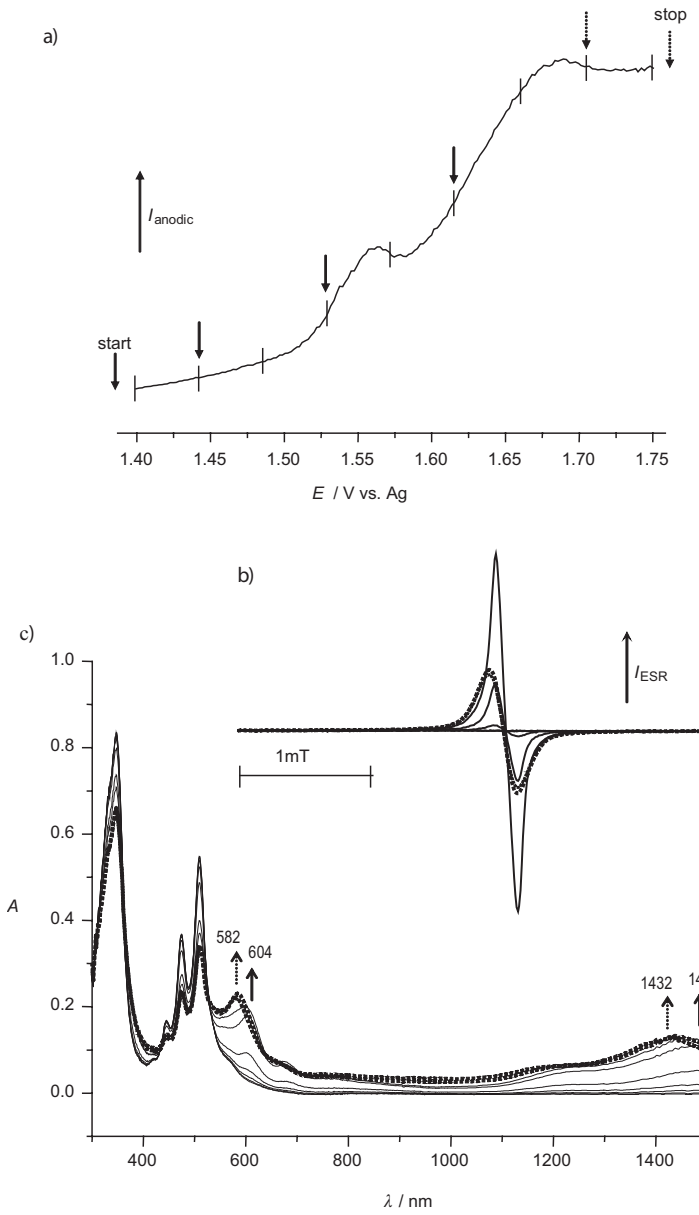

Figure 8. ESR-UV/Vis/NIR spectroelectrochemistry of $\mathbf{A_2}$ deposited on ITO in 0.1 mol L^{-1} $TBABF_4$/ACN. a) In situ voltammetric curve (scan rate: 3 mV s^{-1}). The arrows indicate the potentials at which the ESR spectra (b) were simultaneously measured. The short vertical lines indicate the potentials at which the optical spectra (c) were recorded (dashed lines: the region in which the products produced in the second electron transfer prevail).

vinylene oligomers.[19] To some extent this solid-state behavior is also due to the lower mobility of the molecules.

In the second electron transfer further optical transitions were observed at 582 and 1432 nm with a corresponding decrease in ESR intensity (Figure 8b). This confirms the ESR-silent character of the formed dicationic structures. These two optical bands are very similar to those of the monocation, differing only in a slight blue shift similar to that observed in thin-layer spectroelectrochemistry of $\mathbf{A_3}$. However, similar to fullerene electrochemistry[12] the oxidized or reduced species of $\mathbf{A_2}$ undergoes slow dissolution into acetonitrile, and consequently the spectroelectrochemical responses are determined by both the film surface and the dissolved species. Therefore, the influence of dissolved $\mathbf{A_2}^{\bullet+}$ on the Vis/NIR pattern cannot be excluded. Nevertheless, the spectroelectrochemistry of the solid film in contact with acetonitrile is representative for the solid-state behavior and valid for comparison with solution spectroelectrochemistry.

Conclusion

The redox reactions of thermally stable fluoranthenopyracylene oligomers with extended π conjugation were studied by in situ ESR-UV/Vis/NIR spectroelectrochemistry. They exhibit both reversible reduction (n doping) and oxidation (p doping). One-electron transfer to these structures results in an initial formation of radical ions. In the shortest "oligomers" $\mathbf{A_1}$ and $\mathbf{B_1}$, ESR-silent, doubly charged σ dimers are reversibly formed by a chemical follow-up reaction of the radical anions of $\mathbf{A_1}$ and $\mathbf{B_1}$ and the radical cation of $\mathbf{B_1}$. Compound $\mathbf{B_1}$ is the first for which this dimerization was observed for both the radical anion and the radical cation. While the oxidation of $\mathbf{A_1}$ leads to irreversible formation of its dimers **D1** and **D2**, a slight extension of the π system, as in $\mathbf{B_1}$, results in sufficient stabilization of the radical cation to prevent irreversible dimerization. The larger π systems of $\mathbf{A_2}$–$\mathbf{A_6}$ lead to reversible oxidative and reductive redox behavior and no formation of interchain dimers. Like for oligo(*p*-phenylenevinylene)s the redox potential shifts towards lower energies and the potential difference between subsequent redox states decreases. As the separation of the oxidation potentials of $\mathbf{A_2}$–$\mathbf{A_6}$ is larger than for reduction a stronger Coulombic repulsion between positive charges is expected. An ESR signal (singlet) was detected in the first electron transfer for all structures $\mathbf{A_2}$–$\mathbf{A_6}$ at the first anodic peak. Increasing the chain length decreases the ESR linewidth, and the much

broader NIR spectra of the radical cations indicate high delocalization and mobility of positive charges on the chain. Thin films of $\mathbf{A_1}$ and $\mathbf{A_2}$ on ITO substrates exhibited similar optical and ESR spectroelectrochemical behavior to their solutions. Therefore, both redox behavior and stabilization of charged states are comparable in solution and in the solid state.

Experimental Section

Cyclic voltammograms were obtained in a three-electrode system with platinum working and counterelectrodes and silver-wire pseudoreference electrode. The potentials were corrected against ferrocene/ferrocenium (Fc/Fc^+) internal standard added after each measurement. ESR and optical measurements were carried out in *o*-dichlorobenzene (Aldrich) with 0.1 mol L^{-1} tetrabutylammonium tetrafluoroborate ($TBABF_4$, Fluka) as supporting electrolyte. The ESR spectra were recorded on a 300D X-Band ESR spectrometer (Bruker, Germany), and optical spectra on a UV/Vis/NIR spectrometer system TIDAS (J & M, Aalen, Germany) or UV/Vis spectrometer S 2000 (Sentronic, Germany). A PG 284 potentiostat (HEKA, Germany) was used for potential control.

Compounds $\mathbf{A}_n$ ($n=1$, 2, 4, 6) and $\mathbf{B}_n$ ($n=1$, 2) (Scheme 1) were synthesized using previously reported procedures.[5,20] The sample films were prepared by evaporating the compounds onto ITO-coated glass at 1×10^{-6} mbar in the temperature range from 300 to 500 °C.

Acknowledgement

This work was supported by the DFG (Germany). P.R. thanks Alexander von Humboldt Foundation and Slovak Grand Agency (VEGA 1/0053/03, 1/3579/06) for financial support.

[1] A. Petr, L. Dunsch, A. Neudeck, *J. Electroanal. Chem.* **1996**, *412*, 153–158.
[2] For a review on self-association of radical ions, see T. Nishinaga, K. Komatsu, *Org. Biomol. Chem.* **2005**, *3*, 561–569.
[3] a) I. G. Hill, D. Milliron, J. Schwartz, A. Kahn, *Appl. Surf. Sci.* **2000**, *166*, 354–362; b) K. Seki, N. Hayashi, H. Oji, E. Ito, Y. Ouchi, H. Ishii, *Thin Solid Films* **2001**, *393*, 298–303; c) A. Petr, F. Zhang, H. Peisert, M. Knupfer, L. Dunsch, *Chem. Phys. Lett.* **2004**, *385*, 140–143.
[4] J. Jacob, S. Sax, T. Piok, E. J. W. List, A. C. Grimsdale, K. Müllen, *J. Am. Chem. Soc.* **2004**, *126*, 6987–6995.
[5] a) L. Dunsch, P. Rapta, N. Schulte, A. D. Schlüter, *Angew. Chem.* ***2002****, 114*, 2187–2190; *Angew. Chem. Int. Ed.* **2002**, *41*, 2082–2086; b) see also A. D. Schlüter, *Adv. Mater.* **1991**, *3*, 282–291.
[6] a) M. Ranger, M. Leclerc, *Can. J. Chem. Rev. Can. Chim.* **1998**, *76*, 1571–1577; b) M. Leclerc, *J. Polym. Sci. Polym. Chem.* **2001**, *A39*, 2867–2873.
[7] a) J. D. Debad, J. C. Morris, P. Magnus, A. J. Bard, *J. Org. Chem.* **1997**, *62*, 530–537; b) E. F. Fabrizio, A. Payne, N. E. Westlund, A. J. Bard, P. P. Magnus, *J. Phys. Chem.* **2002**, *106A*, 1961–1968.
[8] A. Reymond, G. K. Fraenkel, *J. Phys. Chem.* **1967**, *71*, 4507.
[9] a) K. Ueno, N. Kitamura, *Analyst* **2003**, *128*, 1401–1405; b) C.-C. Chao, M. Leung, Y. O. Su, K.-Y. Chiu, T.-H. Lin, S.-J. Shieh, S.-C. Lin, *J. Org. Chem.* **2005**, *70*, 4323–4331.
[10] J. Heinze, P. Tschuncky in *Electronic Materials: The Oligomer Approach*, (Eds.: K. Müllen, G. Wegner), Wiley-WCH, Weinheim, **1998**, p. 479.
[11] a) J. A. E. H. van Haare, E. E. Havinga, J. L. J. van Dongen, R. A. J. Janssen, J. Cornil, J.-L. Brédas, *Chem. Eur. J.* **1998**, *4*, 1509–1522; b) V. M. Geskin, J.-L. Brédas, *ChemPhysChem* **2003**, *4*, 498–505.
[12] C. A. Reed, R. D. Bolskar, *Chem. Rev.* **2000**, *100*, 1075–1119.
[13] E. Houze, M. Nechtschein, A. Pron, *Phys. Rev. B56*, 12263–12267.
[14] A. Alberti, B. Ballarin, M. Guerra, D. Macciantelli, A. Mucci, F. Parenti, L. Schenetti, R. Seeber, C. Zanardi, *ChemPhysChem* **2003**, *4*, 1216–1225.
[15] A. Neudeck, L. Kress, *J. Electroanal. Chem.* **1997**, *437*, 141–156.
[16] L. Dunsch, A. Neudeck, P. Rapta, *Fresenius J. Anal. Chem.* **2000**, *367*, 314–319.
[17] P. Rapta, A. Neudeck, A. Petr, L. Dunsch, *J. Chem. Soc. Faraday Trans.* **1998**, *94*, 3625–3630.
[18] K. Xiao, Y. Q. Liu, X. B. Huang, Y. Xu, G. Yu, D. B. Zhu, *J. Phys. Chem.* **2003**, *107B*, 9226–9230.
[19] E. Levillain, J. Roncali, *J. Am. Chem. Soc.* **1999**, *121*, 8760–8765.
[20] W. D. Neudorff, N. Schulte, D. Lentz, A. D. Schlüter, *Org. Lett.* **2001**, *3*, 3115–3118.

Received: August 4, 2005
Revised: November 29, 2005
Published online: January 24, 2006

